scientific reports

OPEN

Reactivity of a model of B$_3$P$_3$-doped nanographene with up to three CO$_2$ molecules

Maxime Ferrer[1,2], Ibon Alkorta [1✉], Jose Elguero[1] & Josep M. Oliva-Enrich[3]

The reactivity of a B$_3$P$_3$-doped hexa-cata-hexabenzocoronene, as a model of nanographene (B$_3$P$_3$-NG), towards carbon dioxide was studied at the DFT M06-2X/6-311++G(3df,3pd)//M06-2X/6-31+G* level of theory. This compound can be classified as a poly-cyclic poly-Frustrated Lewis Pair (FLP) system, as it presents more than one Lewis Acid/Lewis Base pair on its surface, making the capture of several carbon dioxide molecules possible. Two scenarios were considered to fully characterize the capture of CO$_2$ by this multi-FLP system: (i) fixation of three CO$_2$ molecules sequentially one by one; and (ii) simultaneous contact of three CO$_2$ molecules with the B$_3$P$_3$-NG surface. The resulting adducts were analyzed as function of activation barriers and the relative stability of the CO$_2$ capture. A cooperativity effect due to the π-delocalization of the hexa-cata-hexabenzocoronene is observed. The fixation of a CO$_2$ molecule modifies the electronic properties. It enhances the capture of additional CO$_2$ molecules by changing the acidy and basicity of the rest of the boron and phosphorus atoms in the B$_3$P$_3$-NG system.

Carbon dioxide, CO$_2$, is a very stable molecule resulting from the oxidation of mineral carbon or carbon chains in organic molecules. It is the most abundant greenhouse gas emitted by human activities[1–3]. Several small molecules, such as carbenes[4–9], guanidines[10–12] and phosphines[13–16], have been shown to be able to form adducts with CO$_2$. Even though CO$_2$ has been used as potential building block in organic synthesis[17–20] mimicking the photosynthesis of plants, more efforts seem necessary to reduce the impact of the surplus human production of this molecule.

Frustrated Lewis Pair (FLP)[21–23] systems, which are characterized by not being able to form Lewis acid-Lewis base adducts, have shown interesting abilities to activate stable molecules such as CO$_2$, N$_2$ or H$_2$[24–26]. A number of experimental and theoretical studies on the activation and sequestration of CO$_2$ by FLP are available in the literature[27–31].

The structure of a derivative of hexabenzo[a,d,g,j,m,p]coronene or hexa-cata-hexabenzocoronene with N-B atoms in relative *para* positions have been described in the literature[32] and its X-ray structure is available in the CSD[33] (Refcode: FEWKIE) (Fig. 1). Several groups have studied the interaction of nanographene and doped nanographene with CO$_2$, and they only found the formation of non-covalent complexes[34–38]. In these complexes, the CO$_2$ molecule is not activated since it shows geometrical characteristics closed to the ones in the isolated CO$_2$ (C–O bonds around 1.17 Å, O–C–O around 179°).

The potential interaction and activation of carbon dioxide by 5,10-disubstituted dibenzoazaborinines and dibenzophosphaborines intramolecular-FLP was investigated by us recently[39]. It was observed that both were able to interact with CO$_2$ due to their FLP features. However, the dibenzophosphaborine with a P/B couple was found to be more effective, mainly due to the lower delocalization of the phosphorus lone pair into the aromatic rings, and its higher tendency to be hypervalent. Thus, combining our previous research and the structure of FEWKIE, we decided to study the potential used of triphosphatriborahexabenzo [a,d,g,j,m,p]coronene (B$_3$P$_3$-NG in Fig. 1) as potential multi-FLP molecule to capture and activate CO$_2$.

The structure of B$_3$P$_3$-NG (NG : nanographene) can be envisioned as the overlap of 6 dibenzophosphaborines sharing a common side phenyl ring (Fig. 1). In other words, the structure presents 6 B/P pairs. Potentially, up to 12 B/P interaction sites can be found in the molecule if its two faces are non-equivalent. Consequently, the possibility that B$_3$P$_3$-NG interacts and form adducts with up to three CO$_2$ molecules has been examined. Also, the potential cooperativity effects on adducts formation have been explored and interpreted.

[1]Instituto de Química Médica (CSIC), Juan de la Cierva, 3, 28006 Madrid, Spain. [2]Doctoral School, Universidad Autónoma de Madrid, 28049 Madrid, Spain. [3]Instituto de Química-Física Rocasolano (CSIC), Serrano, 119, 28006 Madrid, Spain. ✉email: ibon@iqm.csic.es
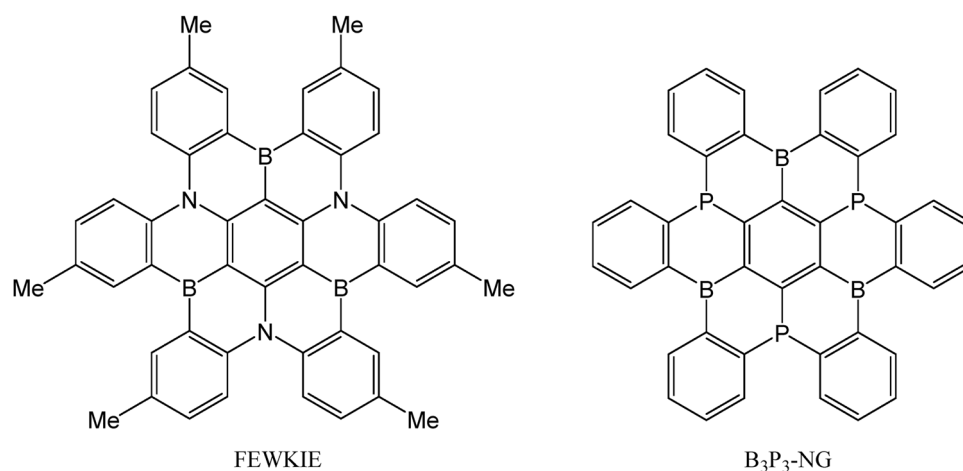
1

Figure 1. Structure of CSD Refcode FEWKIE and the multi-FLP B_3P_3-NG used in this study.

Computational methods

Using the scientific software Gaussian16[40], the structures under study were optimized with the M06-2X DFT functional[41] and the 6-31+G(d) basis set[42]. In order to validate this model, the monomer and one adduct were also optimized at the M06-2X/6-311++G(3df,3pd) level of theory[43]. The calculated root-mean-square deviation (RMSD) between the structures obtained with the M06-2X/6-31+G(d) model and those with the M06-2X/6-311++G(3df,3pd) model was found to be 0.03 Å. In other words, the selected level of theory (M06-2X/6-31+G*) is adequate in order to obtain structures similar to those with the more extended basis set, M06-2X/6-311++G(3df,3pd), at a lower computational cost. The optimized geometries were checked to be minima, no imaginary frequency, or transition states (TS), one imaginary frequency, by means of frequency calculations at M06-2X/6-31+G(d) computational level.

In order to obtain more accurate energies, the electronic energies of all the compounds were recalculated by running single point calculations at the M06-2X/6-311++G(3df,3pd) level of theory using the M06-2X/6-31+G(d) geometries.

The Molecular Electrostatic Potential (MEP) corresponds to the interaction energy between a given molecule and a non-polarizable + 1.0 e positive charge. The MEP enables to localize regions that a priori make a favorable interaction with a positive charge (minima of the MEP) and with a negative one (maxima of the MEP). The MEP of B_3P_3-NG has been calculated on the 0.001 a.u. electron density isosurface to predict the most probable positions to fix the CO_2 molecules. These positions should present a maximum and a minimum, relatively close in space, enabling a double interaction of B_3P_3-NG with one of the nucleophilic oxygens and the electrophilic carbon. These calculations were done using the M06-2X/6-311++G(3df,3pd) model and the Multiwfn software[44].

The topological properties of the electron density for the systems were analyzed by means of the quantum theory of atoms in molecules (QTAIM) model[45,46], implemented in the scientific software AIMAll[47]. The points where the density gradient vanishes are called electron density critical points (CPs). By diagonalizing the Hessian matrix at those points (second derivative matrix of the electron density with respect to electron position), the CPs can be classified depending on the number of non-zero eigenvalues (rank, w) and the sum of the eigenvalues signs (signature, s): CP(w,s). Usually, chemists are interested in the localization of the attractor (3; − 3), bond (3; − 1), ring (3; + 1) and cage critical points (3; + 3). The covalent character of the interactions associated to the bond critical points can be determined by looking at the values of the electron density, the Laplacian, the potential and the kinetic energy density values[48,49]. In the present study, the molecular graphs were computed and plotted with the AIMAll software at the M06-2X/6-311++G(3df,3pd) level of theory.

The non-covalent interactions are generally characterized by a low electron density between the two atoms or group of atoms interacting. A way to characterize the non-covalent interactions of a system is to use the non-covalent interaction index (NCI)[50]. This index enables to localize interaction regions studying the reduced density gradient. A complementary method to identify NCI is the independent gradient model (IGM), implemented in the IGMPlot program[51,52]. This method is based on the difference between the non interacting density gradient and the real density gradient, δG[51,52]. Regions of gradient attenuation indicate the presence of an interaction. Interaction regions are characterized by a positive δG, and the strength of the interactions can be determined by integrating δG into the interaction surface volumes.

In addition, IGMPlot gives the possibility to characterize the strength of a given interaction by calculating its intrinsic bond strength index[53] (IBSI, Eq. 1): the larger the IBSI, the stronger the bond. It is necessary to remember that the IBSI is not linked to a bond order, but to the force constant k of the bond or interaction. Thus, it is an intrinsic dynamic property of the bond.

$$\text{IBSI}_{AB} = \frac{\int_V \frac{\delta G_{AB}}{d_{AB}^2} dV}{\int_V \frac{\delta G_{H_2}}{d_{H_2}^2} dV} \tag{1}$$

The binding energy of adducts and complexes has been calculated as the difference of its energy and the sum of the isolated monomers in their minimum configuration (Eq. 2). In order to evaluate the potential cooperative effect when several molecules of CO_2 interact with B_3P_3-NG, the total binding energy of the adducts has been decomposed (Eq. 3) into a deformation energy of the monomers (E_{def}) (Eq. 4), the two-body interaction energy [$\Delta^2E(ij)$] (Eq. 5) and a cooperative energy (C); E(i) is the energy of the isolated monomer in its minimum energy and E'(i) the energy in the geometry of the complex. Thus, this treatment is similar to the many body energy analysis[54,55] but truncating the expansion in the two-body interaction term and including the higher terms in the cooperativity component.

$$Eb = E(\text{adduct or complex}) - E(B_3P_3\text{-NG}) - n * E(CO_2) \tag{2}$$

$$Eb = E_{def} + E_i + C = \sum E_{def}(i) + \sum \sum \Delta^2E(ij) + C \tag{3}$$

$$E_{def}(i) = E(i) - E'(i) \tag{4}$$

$$\Delta^2E(ij) = E(ij) - E'(i) - E'(j) \tag{5}$$

Finally, the density changes that take place in the systems due to the fixation of the CO_2 molecules, have been analyzed using the Electron Density Shift (EDS) method[56,57]. In a XY complex, the EDS is calculated as the difference between the electron density of the complex and the sum of the isolated monomers in the geometry of the complex (Eq. 6). This method enables to localize regions of space where the density increases by fixation of the CO_2 (EDS > 0) and in the contrary regions where the density decreases (EDS < 0).

$$\text{EDS(r)} = \rho_{XY}(r) - \rho_X(r) - \rho_Y(r) \tag{6}$$

Results and discussion

This section has been divided in four subsections: (3.1) the characteristics of the isolated B_3P_3-NG will be discussed, (3.2) the sequential interaction and incorporation of CO_2 to the B_3P_3-NG molecule, (3.3) the cooperativity analysis of the process described in "Sequential interaction and capture of co2 by b3p3-ng." Section, and (3.4) where three CO_2 molecules will be present along the whole reaction process of interaction and incorporation. The complex and adduct formation of the third molecule is common to the two mechanisms discussed in 3.2 and 3.4, and consequently the global results are the same.

The nomenclature used for the stationary points between B_3P_3-NG and one or more CO_2 molecules uses the following formalism: B_3P_3-NG:mCO$_2$ will indicate a non-covalent complex of B_3P_3-NG and m CO$_2$ molecules. nCO$_2$-(B_3P_3-NG):mCO$_2$ will be used for the non-covalent complex formed between m CO$_2$ molecules and the B_3P_3-NG having already n CO$_2$ molecules covalently bonded on its surface. nCO$_2$-(B_3P_3-NG)/CO$_2$:mCO$_2$ will specify the TS between the non-covalent complex and the adduct of a molecule of CO_2 with m additional non-covalent molecules of CO_2 interacting to B_3P_3-NG and having n CO$_2$ already attached to its surface. Finally nCO$_2$-(B_3P_3-NG) correspond to the adduct formed by the B_3P_3-NG and n CO$_2$ molecules.

Isolated B_3P_3-doped nanographene. The conformational search of B_3P_3-NG provides two minima (Fig. 2). The most stable one, B_3P_3-NG-A, shows a C_3 symmetry with the three lone pairs of the P atoms pointing towards the same direction (+z in Fig. 2), while B_3P_3-NG-B with C_1 symmetry shows two lone pairs of the P atoms in one direction and the other one in the opposite direction. The energy difference between these two structures is 32.0 kJ mol^{-1}. The barrier to convert B_3P_3-NG-A to B_3P_3-NG-B has been calculated to be 72.4 kJ mol^{-1}. Based on the energy difference of the two conformers, a Boltzmann distribution indicates that only B_3P_3-NG-A will be present at room temperature (n$_a$/n$_b$ > 10^5). In the rest of the article only the B_3P_3-NG-A conformation will be considered and simply labelled as B_3P_3-NG.

The molecular electrostatic potential (MEP) of B_3P_3-NG has been calculated (Fig. 3) to identify the potential regions were the CO_2 molecules could interact. We should emphasize that, in general, when a CO_2 molecule is about to interact with a FLP, it first forms an electrostatic complex. Thus, the MEP can give relevant information about preferential positions in the formation of the complex.

Since the molecule presents a C_3 symmetry, the characteristics of the MEP are repeated by a 120° rotation. There are two types of six-membered rings with P/B atom pairs with respect to the MEP:

- Those with a −13.9 kJ mol^{-1} maximum above the center of the ring in the +z direction. This situation corresponds to those six-membered ring with P/B atoms that are almost coplanar with the two surrounding aromatic rings showing an angle between the centroids of the three rings of 174.7° (Fig. 3b)
- Those that do not present a negative maximum between the phosphorus and the boron atoms. In this case, the six-membered ring with P/B atoms is bent with respect to the two adjacent aromatic rings and the angle between the centroids of the three rings is 148.2° in Fig. 3b.
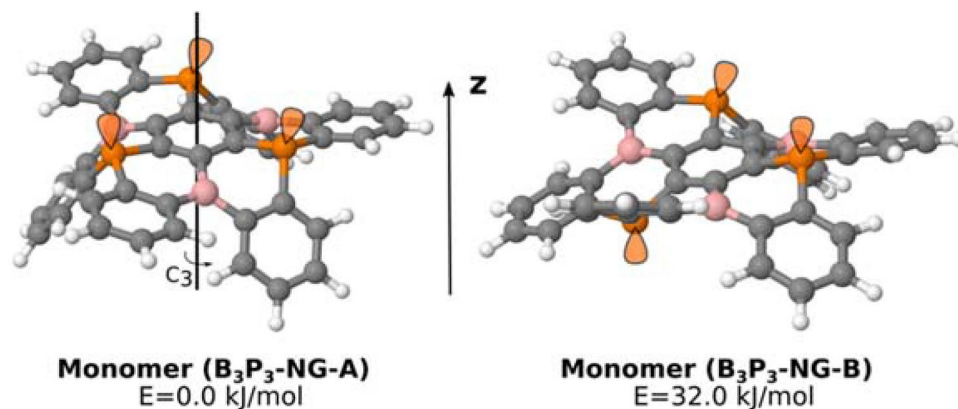
Figure 2. Geometry of the two energy minima found for the B_3P_3-NG monomer optimized at M06-2X/6-31+G* computational level. In orange, schematic orientation of the phosphorus lone pairs.
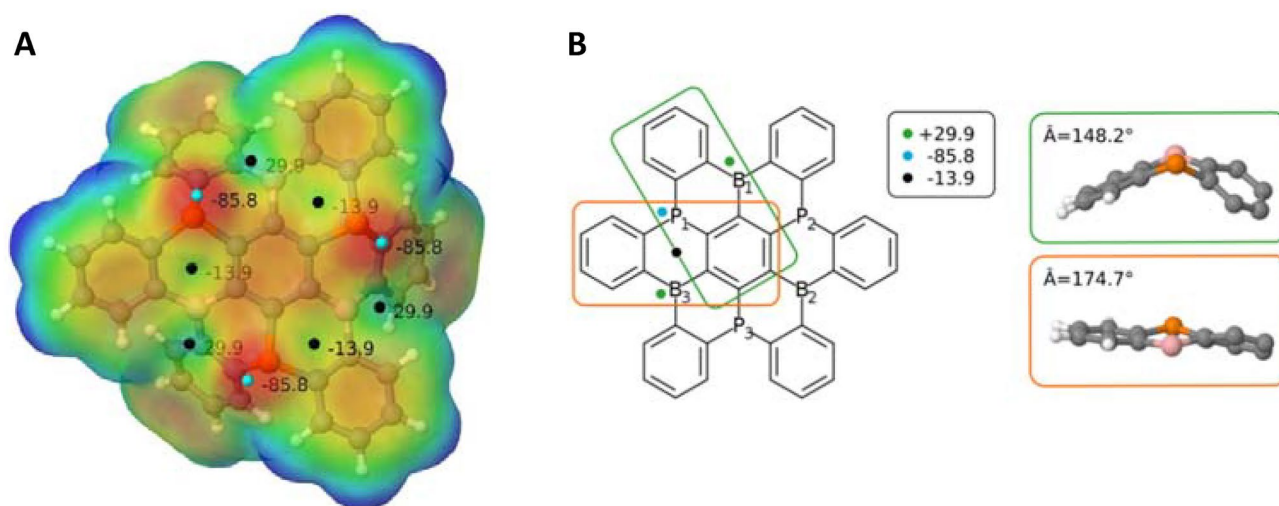

Figure 3. (**A**) MEP of the +z face of monomer B_3P_3-NG on the 0.001 a.u. electronic density isosurface. Cyan small points indicate the minima of the MEP, and black points the corresponding maxima. The MEP values are given in kJ mol^{-1}, the color range used is [−79.0; +66.0] kJ mol^{-1}, M06-2X/6-311++G(3df,3pd)//M06-2X/6-31+G* computations. (**B**) Details of the two types of C_4BP rings in B_3P_3-NG.

As expected, the most favorable position for the interaction of the first CO_2 molecule will be the FLPs that do not have a negative maximum between the Lewis acid and base. This can be at the origin of a repulsive electrostatic interaction with CO_2, with a less favorable formation of the pre-reactive complex. The − z face of B_3P_3-NG (Fig. 2) was not represented as no interesting extrema are located on that face due to the already mentioned orientation of the phosphorus lone pairs pointing towards + z.

Sequential interaction and capture of CO_2 by B_3P_3-NG. As pointed out above, the B_3P_3-NG chosen structure for this study is symmetric, and provides three degenerate favourable positions. In other words, the first adduct can be formed by attacking, without distinction, the pairs P1/B1, P2/B2 or P3/B3 (Fig. 3b).The sequential complex formation and incorporation of CO_2 to the B_3P_3-NG molecule will be discussed below and the energy profile of the process is shown in Fig. 4.

First, as it is often the case when a CO_2 molecule is interacting with a FLP, a pre-reactive complex is formed, in the present case with a binding energy of –20.9 kJ mol^{-1}. In general, the complex is stabilized by electrostatic interactions. Indeed, as it can be observed in Fig. 5A, the CO_2 molecule is not activated. It remains in a geometry close to the one it adopts when isolated in vacuum, with C-O bonds around 1.17 Å and a O–C–O angle around 179°. As indicated in the molecular graph of the $(B_3P_3$-NG):CO_2, Fig. 5A, only one oxygen atom in CO_2 is interacting with the acidic and basic center of B_3P_3-NG. A bond path is observed between the oxygen and the boron atom, as well as between the same oxygen and the phosphorus atom. The density at the BCP for these interactions is 0.009 and 0.008 a.u. respectively. As observed in the case of the dibenzophosphaborine[39], CO_2 is tilted toward the central phenyl ring, due to a π-π stacking between the π-system of the B_3P_3-NG and the C=O double bond. The IGMPlot software was used to characterize the interaction between the B_3P_3-NG and the CO_2 molecules
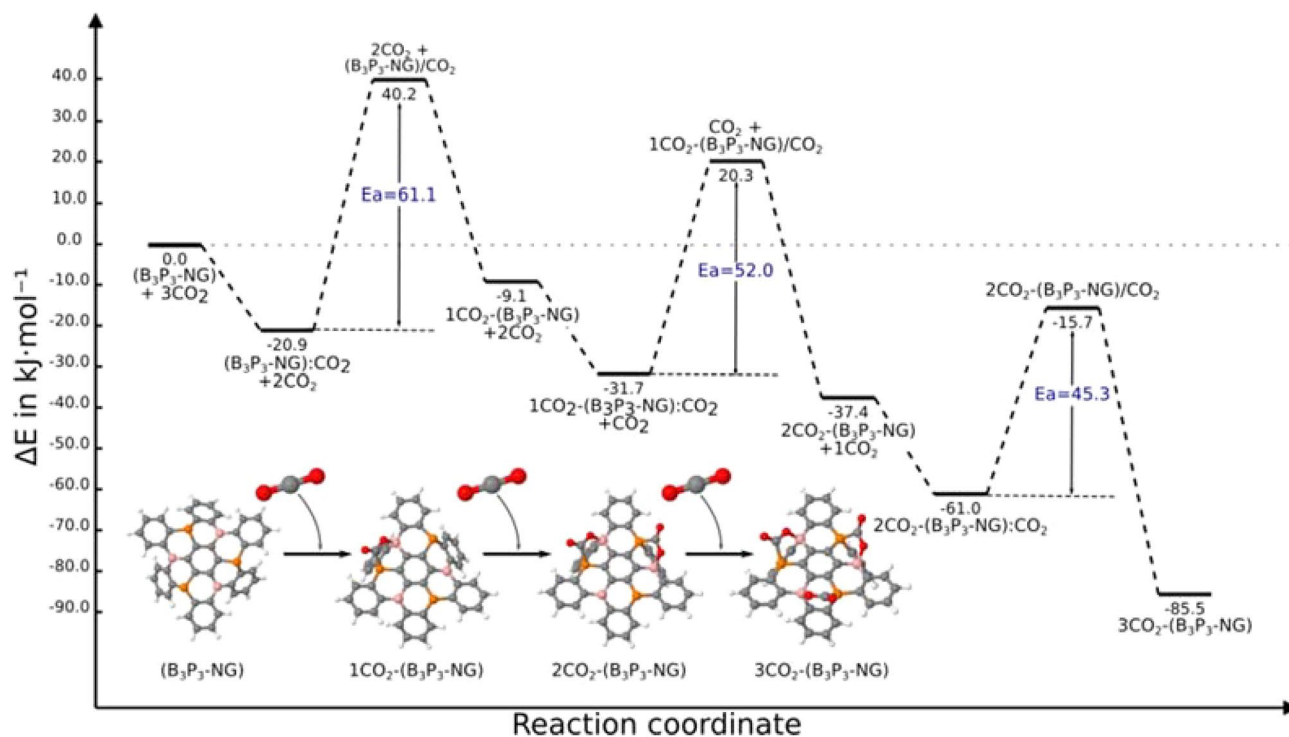
Figure 4. Reaction profile of the sequential capture of three CO_2 molecules by B_3P_3-NG. The energies are in kJ mol^{-1} and correspond to M06-2X/6-311++G(3df,3pd)//M06-2X/6-31+G* calculations.
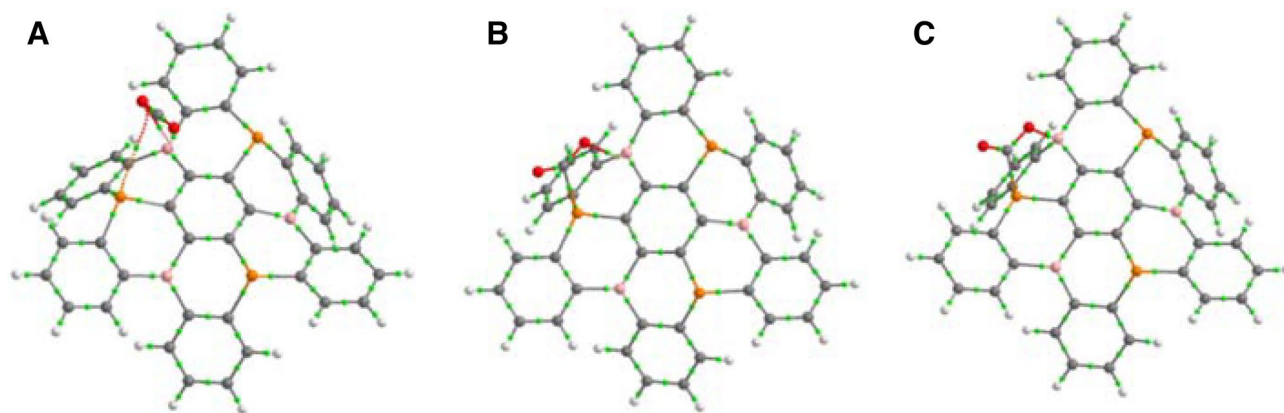

Figure 5. Molecular graph of the (**A**) (B_3P_3-NG):CO_2 , (**B**) (B_3P_3-NG)/CO_2 and (**C**) $1CO_2$-(B_3P_3-NG) of the first CO_2 capture by B_3P_3-NG. Bond critical points (BCP) are shown in green.

in the complex. The interaction surface between B_3P_3-NG (Fragment 1) and CO_2 (Fragment 2) is depicted in Fig. 6, using a density cutoff of 0.01 a.u. It can be observed that the orientation of the CO_2 molecule is linked with a maximization of the π-π staking between the π-system of the P/B ring and the double bonds of CO_2. These interactions appear for a density of 0.008 a.u.. The attractive interaction [sign($λ_2$) ρ = − 0.008 a.u.], has a larger maximum value, hence a higher contribution as compared to the repulsive interaction [sign($λ_2$) ρ = + 0.008 a.u.].

Also a non-covalent complex between the B1/P2 couple of B_3P_3-NG and CO_2 has been obtained with a binding energy of −20.7 kJ mol^{-1} (almost the same energy as B_3P_3-NG:$1CO_2$). However all attempts to optimize the corresponding adduct in that position failed, returning back to the complex in the optimization process. The P–C and B–O distances in this less favorable B1/P2 complex are longer than the ones in the complex with the B1/P1 pair (d(P2–C) = 3.979 Å vs. d(P1–C) = 3.332 Å; d(B1–O) = 2.955 Å vs. d(B1–O) = 2.886 Å).

The transformation of the first pre-reactive complex into the adduct proceeds through a TS with an energy barrier of + 40.2 kJ mol^{-1} (Fig. 5B). The adduct has a relative energy of − 9.1 kJ mol^{-1} with respect to the isolated B_3P_3-NG and CO_2 molecules (Fig. 5C). It is more stable than the entrance channel (B_3P_3-NG + CO_2) but less stable than the complex. This behavior is common in the interaction between CO_2 and FLPs[31,39,58].

The formation of the adduct breaks the symmetry of the system. The remaining P/B couples are no longer equivalent by symmetry. For example, in the case of the B2/P2 pair the two surrounding aromatic rings show
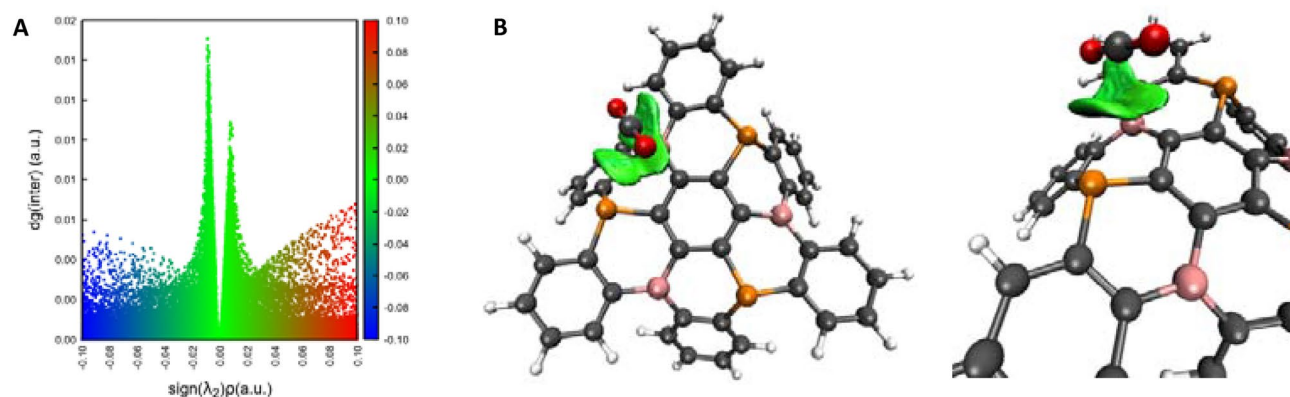
Figure 6. IGMPlot results of $(B_3P_3\text{-NG}):CO_2$. (**A**) 2D plot of the δg as a function of the $\text{sign}(\lambda_2)$. Attractive interactions, Van der Waals regions, and repulsive interactions are shown in blue, green and red colours respecitvely. (**B**) Interaction surface of the CO_2 molecule with the π system of B_3P_3-NG.

an angle between the centroids of the three rings of 146.4° ; this angle is 151.9° in the case of the P3/B3 pair. The MEP of the P/B pairs is also different. For the P2/B2 pair (Fig. S1 of the Supporting Material), the extrema are respectively − 111.6 and + 31.8 kJ mol⁻¹. For the P3/B3 pair, the extrema are − 78.5 and + 72.5 kJ mol⁻¹. The adduct in both cases are identical but the differences can influence the stability of the TSs. A priori, it is not possible to predict which FLP will provide the smaller barrier to fix the new CO_2 molecule. Indeed, P2/B2 has a more adequate geometry, but B2 is less electrophilic than B3. However, P2 is more nucleophilic than P3 based on the MEP. The TS which enables the fixation of the CO_2 molecule on the P2/B2 FLP has a relative energy of + 20.3 kJ mol⁻¹ and the one where CO_2 interacts with P3/B3 is approximately 5 kJ mol⁻¹ higher in energy. Thus, the fixation of the new CO_2 molecule is easier on the P2/B2 pair for kinetic reasons. Statistically, both reactions can take place, but in this work we will consider only the most probable based on its lower barrier.

Finally, the last CO_2 molecule can be fixed on the remaining P3/B3 pair. The TS $2CO_2$-(B_3P_3-NG)/CO_2 has a relative energy of − 15.7 kJ mol⁻¹ with respect to the isolated systems and the $3CO_2$-(B_3P_3-NG) has a relative energy of − 85.5 kJ mol⁻¹. The striking point with this last capture is that the TS is more stable than the entrance channel.

In order to get more insights into the reaction, the enthalpies and free energies of the successive captures were calculated (Fig. S2). As expected, the entropic term, −TΔS, has a large positive contribution, since two molecules react to form only one. For that reason, at room temperature, the captures, even if the last two are exothermic, will not be spontaneous. One can however observe a cooperative effect as the ΔΔG reduces when increasing the number of CO_2 molecules captured (28.6; 16.6; 3.2 kJ mol⁻¹).

Understanding the cooperativity along the reaction. The presence of a cooperative effect is clear, as observed in Fig. 4. On one hand the adducts are more stable, but strikingly the activation barriers are reduced with the number of captured CO_2 molecules.

Stability of the adducts. The first indication of cooperativity is that the larger the number of CO_2 molecules on the B_3P_3-NG structure, the more stable the obtained adducts are. The increase in the interaction energy and the presence of a cooperative effect is even more obvious by using the decomposition scheme proposed in the Computational Methods section. A priori, the increase in stability can be related to an increase of the interaction energy between the CO_2 and the B_3P_3-NG, and/or a decrease of the deformation energy needed to form the adduct. The interaction energy in the adduct per CO_2 molecule (E_i/nCO_2), ranges from − 415.3 kJ mol⁻¹ in $1CO_2$-(B_3P_3-NG) to − 437.5 kJ mol⁻¹ in $2CO_2$-(B_3P_3-NG) adduct/complex and − 457.9 kJ mol⁻¹ in the $3CO_2$-(B_3P_3-NG) one (Table 1). The deformation energy of B_3P_3-NG per CO_2 molecule increases slightly with the number of CO_2 molecules: 151.8 kJ mol⁻¹, 155.1 kJ mol⁻¹ and 155.3 kJ mol⁻¹ for 1, 2 and 3 CO_2 molecules, respectively. Thus, it seems that the increase in adduct stability is mainly due to an increase of interaction energy between CO_2 and the B_3P_3-NG moiety. It can be realized that indeed, the interaction energy by CO_2 increases, but that the total increase in stability is due to the presence of a cooperative energy, C. In other words, in the $2CO_2$-(B_3P_3-NG) adduct, the interaction energy of $CO_2(1)$ and $CO_2(2)$ is larger than the one of $CO_2(1)$ in the $1CO_2$-(B_3P_3-NG) adduct. However the presence of $CO_2(1)$ and $CO_2(2)$ at the same time on the B_3P_3-NG induces an extra interaction of –24.1 kJ mol⁻¹, explaining the extra stabilization of the adduct.

The variation in the interaction energy can also be analyzed from a geometrical point of view by looking at the B–O and P–C bonds of the first fixed CO_2 molecule when increasing the number of CO_2 molecules. First, it can be observed that the P1–C distance increases a little bit when adding more CO_2 molecules (Table 2). The total change is 0.006 Å. The B1–O bond is more affected by the fixation of new CO_2 molecules as its distance decreases. It shortens by 0.021 Å, from 1.581 Å in $1CO_2$-(B_3P_3-NG), to 1.574 Å in $2CO_2$-(B_3P_3-NG), to 1.560 Å in $3CO_2$-(B_3P_3-NG) (Table 2). Looking at the IBSI and at the density at the different BCP, it can be observed that the properties of the P–C bonds do not change significantly with the number of attached CO_2 molecules. The strength and the density of this bond are not really influenced by the fixation of new CO_2 molecules. On

	1CO$_2$-(B$_3$P$_3$-NG)	2CO$_2$-(B$_3$P$_3$-NG)	3CO$_2$-(B$_3$P$_3$-NG)
E$_b$			
E$_{def}$	+406.2	+837.6	+1288.2
E$_i$	−415.3	−850.9	−293.3
C		−24.1	−80.4
Total	−9.1	−37.4	−85.5
E$_{def}$			
E$_{def}$ (B$_3$P$_3$-NG)	+151.8	+310.1	+465.9
E$_{def}$ (CO$_2$(1))	+254.4	+263.0	+274.1
E$_{def}$ (CO$_2$(2))		+264.5	+274.1
E$_{def}$ (CO$_2$(3))			+274.1
E$_i$			
E$_i$/nCO$_2$	−415.3	−437.5	−457.9
E$_i$ (B$_3$P$_3$-NG-CO$_2$(1))	−415.3	−420.6	−431.2
E$_i$ (B$_3$P$_3$-NG-CO$_2$(2))		−430.4	−431.2
E$_i$ (B$_3$P$_3$-NG-CO$_2$(3))			−431.2

Table 1. Binding energy (Eb), total and individual deformation energies (E$_{def}$), total interaction energy (E$_i$), interaction energy for each individual contact with a CO$_2$ molecule (Ei$_{B3P3-NG-CO2(n)}$), mean interaction energy per CO$_2$ molecule (E$_i$/nCO$_2$), cooperative energy (C) in kJ mol^{-1} for the different adducts obtained (M06-2X/6-311++G(3df,3pd)//M06-2X/6-31+G*).

	1CO$_2$-(B$_3$P$_3$-NG)			2CO$_2$-(B$_3$P$_3$-NG)			3CO$_2$-(B$_3$P$_3$-NG)		
	Bond distance	IBSI	ρ$_{BCP}$	Bond distance (Å)	IBSI (a.u.)	ρ$_{BCP}$ (a.u.)	Bond distance (Å)	IBSI (a.u.)	ρ$_{BCP}$ (a.u.)
P1–C bond	1.901	0.458	0.160	1.903	0.454	0.159	1.907	0.464	0.158
O–B1 bond	1.581	0.572	0.112	1.574	0.582	0.115	1.560	0.618	0.120

Table 2. Bond distances (Å), intrinsic bond strength index (IBSI) in a.u. and density at the Bond Critical Points (BCP) in a.u. of the P1-C and O-B1 bond in the different adducts. The IBSI were obtained using IGMPlot, and the BCP were localized with AIMAll at M06-2X/6-311++G(3df,3pd)//M06-2X/6-31+G* computational level.

the contrary, it can be observed that the B–O bond gets stronger when increasing the number of CO$_2$ fixed. In other words, it seems that the increase of stability observed is linked with a strengthening of the B-O interaction.

The stabilization of the TSs. As it can be observed in Fig. 4, the successive fixation of CO$_2$ molecules is accompanied by a decrease of the activation barrier. In a previous paper, we observed that during the capture of CO$_2$ by a P/B cyclic FLP, the energy of the TS can be influenced by the basicity of the phosphorus atom[39]. In order to see if the differences in activation energy are related to the increase of phosphorus basicity, we computed Electron Density Shift (EDS) plots of the 1CO$_2$-(B$_3$P$_3$-NG) and 2CO$_2$-(B$_3$P$_3$-NG) adducts, as shown in Fig. 7.

As it can be observed, the fixation of the first CO$_2$ molecule in P1/B1 induces a shift of the density toward the phosphorus atoms (P2) while the rest of the system is not influenced by CO$_2$ addition (Fig. 7A). The same behavior is observed when 2CO$_2$-(B$_3$P$_3$-NG) is formed (Fig. 7B).

Simultaneous reaction of three CO$_2$ molecules with B$_3$P$_3$-NG. Another alternative is B$_3$P$_3$-NG surrounded by CO$_2$ molecules as the addition reactions proceed. These conditions can occur in a CO$_2$ atmosphere or CO$_2$ supercritical. Thus, we consider the presence of three CO$_2$ molecules along the reaction coordinate, as depicted in Fig. 8.

We should emphasize that in this new reaction path (Fig. 8, orange curve), the pre-reactive complexes of the next step and adducts from the previous step are the same stationary points. For this reason the new path presents only 7 stationary points instead of 9, as describe above in "Isolated B3P3-doped nanographene" Section.

The first stationary point, (B$_3$P$_3$-NG):3CO$_2$, has a relative energy of −65.1 kJ mol^{-1} while the (B$_3$P$_3$-NG):CO$_2$ adduct/complex is −20.9 kJ mol^{-1}. In other words, the presence of the two extra CO$_2$ molecules in (B$_3$P$_3$-NG):3CO$_2$ produces a stabilization of −44.2 kJ mol^{-1}, more than twice the energy of (B$_3$P$_3$-NG):CO$_2$, hence the presence of a cooperativity effect; otherwise the energy of (B$_3$P$_3$-NG):3CO$_2$ would have been three times the energy of (B$_3$P$_3$-NG):CO$_2$.

We also used the IGMPlot software in order to study this cooperative effect. By integrating the peaks corresponding to the attractive weak interactions, we obtained a value of 0.09 a.u. for (B$_3$P$_3$-NG):CO$_2$ with a rise
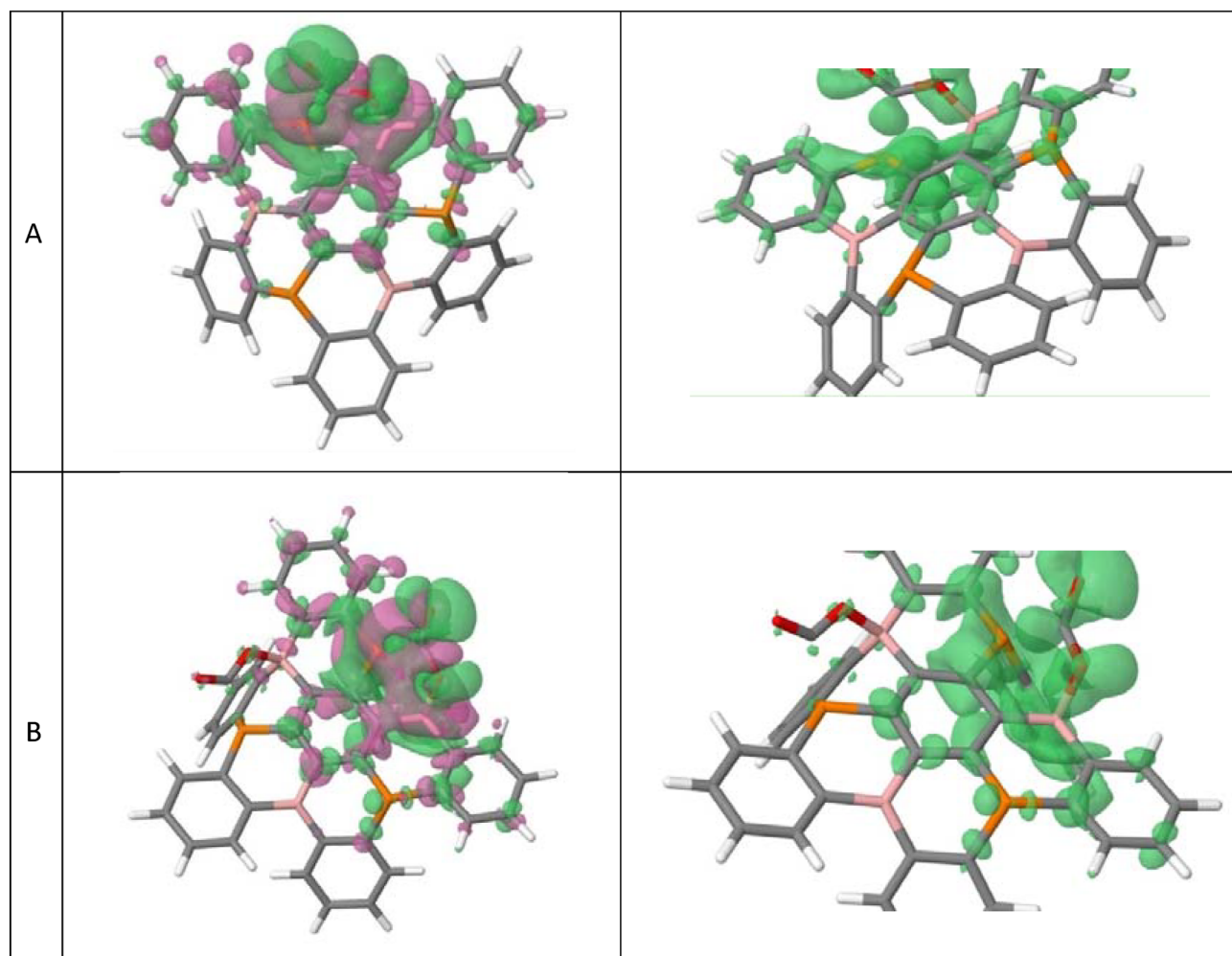
Figure 7. Electron Density Shift (EDS) plots of (**A**) $1CO_2$-$(B_3P_3$-NG) and (**B**) $2CO_2$-$(B_3P_3$-NG) . In magenta color the region of electron density decrease and in green the region of electron density increase. An isovalue of 0.001 a.u. was used for the plot.

of 0.36 a.u. for $(B_3P_3$-NG):$3CO_2$, more than three times larger, confirming the cooperativity effect as more CO_2 molecules are added to the system.

In this new reaction profile one can observe that all TS are more stable as compared to the entrance channel. The relative energy of the first TS ranges from $+40.2$ to -4.3 kJ mol^{-1} ($\Delta E = 44.5$ kJ mol^{-1}), and the second TS ranges from $+20.3$ to -2.7 kJ mol^{-1} ($\Delta E = 23.0$ kJ mol^{-1}). It can be pointed out that the activation energies are similar in both reaction paths (61.1 vs. 60.8 kJ mol^{-1} and 52.0 vs. 51.9 kJ mol^{-1}). This fact is due to the similar stabilization of adducts and TSs.

Conclusion

The capture of CO_2 molecules by the B_3P_3-NG compound was studied by means of DFT computational methods. Two potential mechanisms have been studied: (i) the interaction between B_3P_3-NG and CO_2 molecules and adduct formation is done sequentially, and (ii) three CO_2 molecules interact simultaneously with the B_3P_3-NG compound along the reaction coordinate.

The main conclusions are:

- The capture of CO_2 by B_3P_3-NG presents a cooperative effect.
- The increase in number of CO_2 molecules fixed on the B_3P_3-NG surface stabilizes the respective adducts due to an increase of the boron acidity, and then an increase of the boron-oxygen interaction.
- The decrease of the activation barriers with the number of CO_2 molecules is due to a basicity increase of the phosphorus.
- The cooperative effects observed in this system are linked to the π delocalization of the system. The modifications imposed by the fixation of a new CO_2 molecule are compensated by a π-electron reorganization, affecting the acidity and basicity of the boron and phosphorus atoms.
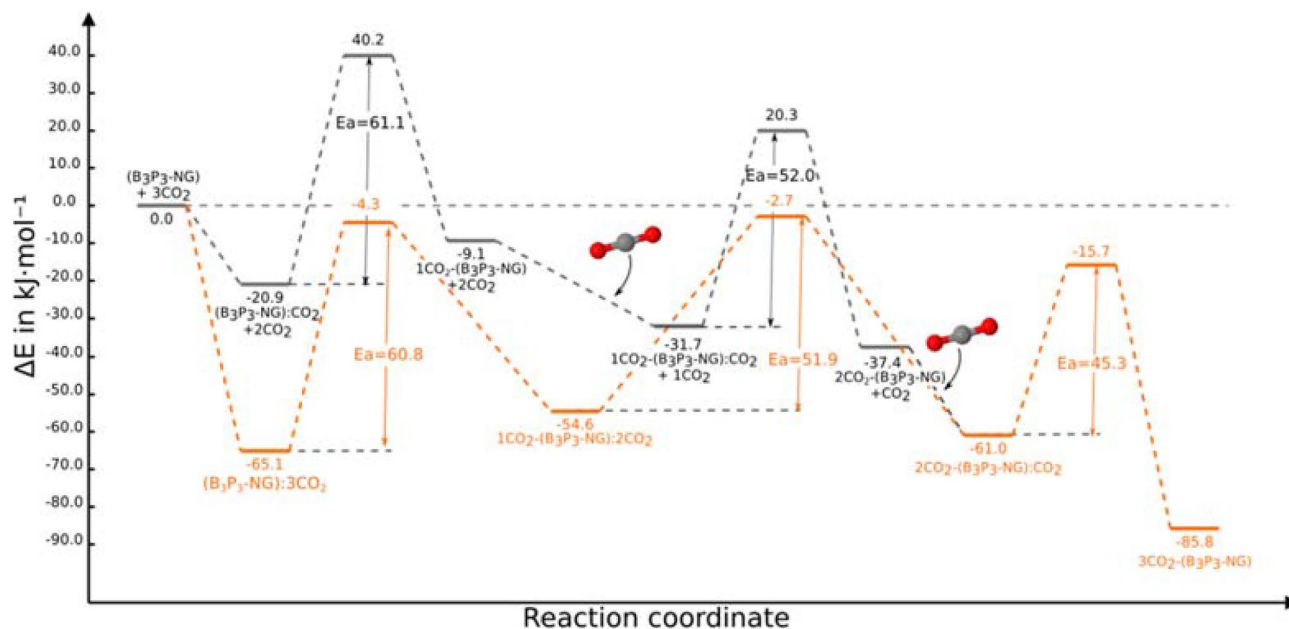
Figure 8. Comparison of the reaction profiles obtained by sequential addition of CO_2 molecules (black), and with 3 CO_2 molecules along the reaction profile (orange). The energies are in kJ mol^{-1} and calculated at M06-2X/6-311++G(3df,3pd)//M06-2X/6-31+G* computational level.

- The multi-capture can be enhanced by considering that several CO_2 molecules are simultaneously in contact with the B_3P_3-NG surface.

Data availability
All data generated or analysed during this study are included in this published article and its supplementary information files.

References
1. Nejat, P., Jomehzadeh, F., Taheri, M. M., Gohari, M. & Abd. Majid, M. Z. A global review of energy consumption, CO_2 emissions and policy in the residential sector (with an overview of the top ten CO_2 emitting countries). *Renew. Sustain. Energ. Rev.* **43**, 843–862. https://doi.org/10.1016/j.rser.2014.11.066 (2015).
2. Kijewska, A. & Bluszcz, A. Analysis of greenhouse gas emissions in the European Union member states with the use of an agglomeration algorithm. *J. Sustain. Mining* **15**, 133–142. https://doi.org/10.1016/j.jsm.2017.02.001 (2016).
3. Xu, J., Zhou, M. & Li, H. The drag effect of coal consumption on economic growth in China during 1953–2013. *Resour. Conserv. Recycl.* **129**, 326–332. https://doi.org/10.1016/j.resconrec.2016.08.027 (2018).
4. Kuhn, N., Steimann, M. & Weyers, G. Synthese und eigenschaften von 1,3-diisopropyl-4,5-dimethylimidazolium-2-carboxylat. Ein stabiles Carben-Addukt des Kohlendioxids [1]/Synthesis and Properties of 1,3-Diisopropyl-4,5-dimethylimidazolium-2-carboxylate. *Stable Carbene Adduct Carbon Dioxide [1]* **54**, 427–433. https://doi.org/10.1515/znb-1999-0401 (1999).
5. Duong, H. A., Tekavec, T. N., Arif, A. M. & Louie, J. Reversible carboxylation of N-heterocyclic carbenes. *Chem. Commun.* https://doi.org/10.1039/B311350G (2004).
6. Kayaki, Y., Yamamoto, M. & Ikariya, T. N-heterocyclic carbenes as efficient organocatalysts for CO_2 fixation reactions. *Angew. Chem. Int. Ed.* **48**, 4194–4197. https://doi.org/10.1002/anie.200901399 (2009).
7. Wang, S. & Wang, X. Imidazolium ionic liquids, imidazolylidene heterocyclic carbenes, and zeolitic imidazolate frameworks for CO_2 capture and photochemical reduction. *Angew. Chem. Int. Ed.* **55**, 2308–2320. https://doi.org/10.1002/anie.201507145 (2016).
8. Alkorta, I., Montero-Campillo, M. M. & Elguero, J. Trapping CO_2 by adduct formation with nitrogen heterocyclic carbenes (NHCs): A theoretical study. *Chem. Eur. J.* **23**, 10604–10609. https://doi.org/10.1002/chem.201701444 (2017).
9. Montero-Campillo, M. M., Alkorta, I. & Elguero, J. Binding indirect greenhouse gases OCS and CS 2 by nitrogen heterocyclic carbenes (NHCs). *PCCP* **20**, 19552–19559. https://doi.org/10.1039/C8CP03217C (2018).
10. Villiers, C., Dognon, J.-P., Pollet, R., Thuéry, P. & Ephritikhine, M. An isolated CO_2 adduct of a nitrogen base: Crystal and electronic structures. *Angew. Chem. Int. Ed.* **49**, 3465–3468. https://doi.org/10.1002/anie.201001035 (2010).
11. Santo, R. D. d. E., Capitão, R. M. & González, E. R. P. in *Guanidines as Reagents and Catalysts II* (ed Philipp Selig) 27–74 (Springer International Publishing, 2017).
12. Anila, S. & Suresh, C. H. Guanidine as a strong CO_2 adsorbent: A DFT study on cooperative CO_2 adsorption. *PCCP* **23**, 13662–13671. https://doi.org/10.1039/D1CP00754H (2021).
13. Buß, F., Mehlmann, P., Mück-Lichtenfeld, C., Bergander, K. & Dielmann, F. Reversible carbon dioxide binding by simple Lewis base adducts with electron-rich phosphines. *J. Am. Chem. Soc.* **138**, 1840–1843. https://doi.org/10.1021/jacs.5b13116 (2016).
14. Mehlmann, P., Mück-Lichtenfeld, C., Tan, T. T. Y. & Dielmann, F. Tris(imidazolin-2-ylidenamino)phosphine: A crystalline phosphorus(III) superbase that splits carbon dioxide. *Chem. Eur. J.* **23**, 5929–5933. https://doi.org/10.1002/chem.201604971 (2017).
15. Alkorta, I., Trujillo, C., Sánchez-Sanz, G. & Elguero, J. Solvent and substituent effects on the phosphine + CO_2 reaction. *Inorganics* https://doi.org/10.3390/inorganics6040110 (2018).

16. Sánchez-Sanz, G., Alkorta, I., Elguero, J. & Trujillo, C. Sequestration of CO_2 by phosphatrane molecules. *ChemPhysChem* **20**, 3195–3200. https://doi.org/10.1002/cphc.201900905 (2019).

17. Liu, Q., Wu, L., Jackstell, R. & Beller, M. Using carbon dioxide as a building block in organic synthesis. *Nat. Commun.* **6**, 5933. https://doi.org/10.1038/ncomms6933 (2015).

18. Artz, J. *et al.* Sustainable conversion of carbon dioxide: An integrated review of catalysis and life cycle assessment. *Chem. Rev.* **118**, 434–504. https://doi.org/10.1021/acs.chemrev.7b00435 (2018).

19. Dabral, S. & Schaub, T. The use of carbon dioxide (CO_2) as a building block in organic synthesis from an industrial perspective. *Adv. Synth. Catal.* **361**, 223–246. https://doi.org/10.1002/adsc.201801215 (2019).

20. Das, S. *CO2 as a Building Block in Organic Synthesis* (WILEY-VCH GmbH, 2020).

21. Erker, G. & Stephan, D. W. *Frustrated Lewis Pairs I. Uncovering and Understanding* Vol. 332 (Springer, 2013).

22. Erker, G. & Stephan, D. W. *Frustrated Lewis Pairs II. Expanding the Scope* Vol. 334 (Springer, 2013).

23. Slootweg, J. C. & Jupp, A. R. *Frustrated Lewis Pairs* (Springer, 2021).

24. Travis, A. L. *et al.* Small molecule activation by frustrated Lewis pairs. *Dalton Trans.* **42**, 2431–2437. https://doi.org/10.1039/C2DT32525J (2013).

25. Kehr, G. & Erker, G. Frustrated Lewis pair chemistry: Searching for new reactions. *Chem. Rec.* **17**, 803–815. https://doi.org/10.1002/TCR.201700010 (2017).

26. Pal, R., Ghara, M. & Chattaraj, P. K. Activation of small molecules and hydrogenation of CO_2 catalyzed by frustrated Lewis pairs. *Catalysts* **12**, 201. https://doi.org/10.3390/catal12020201 (2022).

27. Sharma, G., Newman, P. D. & Platts, J. A. A review of quantum chemical studies of frustrated Lewis pairs. *J. Mol. Graph. Modell.* **105**, 107846. https://doi.org/10.1016/j.jmgm.2021.107846 (2021).

28. Zhuang, D., Rouf, A. M., Li, Y., Dai, C. & Zhu, J. Aromaticity-promoted CO2 capture by P/N-based frustrated Lewis pairs: A theoretical study. *Chem.: Asian J.* **15**, 266–272. https://doi.org/10.1002/asia.201901415 (2020).

29. Soroudi, S. & Kassaee, M. Z. Capture of CO_2 by novel diiodo-N, N-imidazoliumvinylidene: A theoretical quest. *J. Phys. Org. Chem.* **35**, e4323. https://doi.org/10.1002/poc.4323 (2022).

30. von Wolff, N., Lefèvre, G., Berthet, J. C., Thuéry, P. & Cantat, T. Implications of CO_2 activation by frustrated Lewis pairs in the catalytic hydroboration of CO_2: A view using N/Si+ frustrated Lewis pairs. *ACS Catal.* **6**, 4526–4535. https://doi.org/10.1021/acscatal.6b00421 (2016).

31. Ferrer, M., Alkorta, I., Elguero, J. & Oliva-Enrich, J. M. Sequestration of carbon dioxide with frustrated Lewis pairs based on N-heterocycles with silane/germane groups. *J. Phys. Chem. A* **125**, 6976–6984. https://doi.org/10.1021/acs.jpca.1c04787 (2021).

32. Matsui, K. *et al.* One-shot multiple borylation toward BN-doped nanographenes. *J. Am. Chem. Soc.* **140**, 1195–1198. https://doi.org/10.1021/jacs.7b10578 (2018).

33. Groom, C. R., Bruno, I. J., Lightfoot, M. P. & Ward, S. C. The Cambridge structural database. *Acta Crystallogr. B* **72**, 171–179. https://doi.org/10.1107/S2052520616003954 (2016).

34. Babar, V., Sharma, S. & Schwingenschlögl, U. Gas sensing performance of pristine and monovacant C6BN monolayers evaluated by density functional theory and the nonequilibrium green's function formalism. *J. Phys. Chem. C* **124**, 5853–5860. https://doi.org/10.1021/acs.jpcc.9b10553 (2020).

35. Salari, A. A. Detection of NO_2 by hexa-peri-hexabenzocoronene nanographene: A DFT study. *C. R. Chim.* **20**, 758–764. https://doi.org/10.1016/j.crci.2017.01.002 (2017).

36. Saha, D., Nelson, K., Chen, J., Lu, Y. & Ozcan, S. Adsorption of CO_2, CH4, and N2 in micro-mesoporous nanographene: A comparative study. *J. Chem. Eng. Data* **60**, 2636–2645. https://doi.org/10.1021/acs.jced.5b00291 (2015).

37. Wang, G. *et al.* A Monolayer composite of h-BN doped by a nano graphene domain: As sensitive material for SO_2 gas detection. *IEEE Electron Device Lett.* **41**, 1404–1407. https://doi.org/10.1109/LED.2020.3008556 (2020).

38. Balasubramanian, R. & Chowdhury, S. Recent advances and progress in the development of graphene-based adsorbents for CO2 capture. *J. Mater. Chem. A* **3**, 21968–21989. https://doi.org/10.1039/C5TA04822B (2015).

39. Ferrer, M., Alkorta, I., Elguero, J. & Oliva-Enrich, J. M. Use of 5,10-disubstituted dibenzoazaborines and dibenzophosphaborines as cyclic supports of frustrated Lewis pairs for the capture of CO_2. *ChemPhysChem* **23**, e202200204. https://doi.org/10.1002/cphc.202200204 (2022).

40. Gaussian 16 Rev. A.03 (Wallingford, CT, 2016).

41. Zhao, Y. & Truhlar, D. G. The M06 suite of density functionals for main group thermochemistry, thermochemical kinetics, noncovalent interactions, excited states, and transition elements: Two new functionals and systematic testing of four M06-class functionals and 12 other functionals. *Theor. Chem. Acc.* **120**, 215–241. https://doi.org/10.1007/s00214-007-0310-x (2008).

42. Hariharan, P. C. & Pople, J. A. The influence of polarization functions on molecular orbital hydrogenation energies. *Theoret. Chim. Acta* **28**, 213–222. https://doi.org/10.1007/BF00533485 (1973).

43. Frisch, M. J., Pople, J. A. & Binkley, J. S. Self-consistent molecular orbital methods 25. Supplementary functions for Gaussian basis sets. *J. Chem. Phys.* **80**, 3265–3269. https://doi.org/10.1063/1.447079 (1984).

44. Lu, T. & Chen, F. Multiwfn: A multifunctional wavefunction analyzer. *J. Comput. Chem.* **33**, 580–592. https://doi.org/10.1002/jcc.22885 (2012).

45. Bader, R. F. W. *Atoms In Molecules: A Quantum Theory* (Clarendon Pr., NewYork, 1990).

46. Popelier, P. L. A. *Atoms In Molecules. An introduction* (Prentice Hall, 2000).

47. Keith, T. A. (2019).

48. Rozas, I., Alkorta, I. & Elguero, J. Behavior of Ylides containing N, O, and C atoms as hydrogen bond acceptors. *J. Am. Chem. Soc.* **122**, 11154–11161. https://doi.org/10.1021/ja0017864 (2000).

49. Espinosa, E., Alkorta, I., Elguero, J. & Molins, E. From weak to strong interactions: A comprehensive analysis of the topological and energetic properties of the electron density distribution involving X-H···F–Y systems. *J. Chem. Phys.* **117**, 5529–5542. https://doi.org/10.1063/1.1501133 (2002).

50. Contreras-García, J. *et al.* NCIPLOT: A program for plotting noncovalent interaction regions. *J. Chem. Theory Comput.* **7**, 625–632. https://doi.org/10.1021/ct100641a (2011).

51. Lefebvre, C. *et al.* The independent gradient model: A new approach for probing strong and weak interactions in molecules from wave function calculations. *ChemPhysChem* **19**, 724–735. https://doi.org/10.1002/cphc.201701325 (2018).

52. Lefebvre, C. *et al.* Accurately extracting the signature of intermolecular interactions present in the NCI plot of the reduced density gradient versus electron density. *PCCP* **19**, 17928–17936. https://doi.org/10.1039/C7CP02110K (2017).

53. Klein, J. *et al.* New way for probing bond strength. *J. Phys. Chem. A* **124**, 1850–1860. https://doi.org/10.1021/acs.jpca.9b09845 (2020).

54. Hankins, D., Moskowitz, J. W. & Stillinger, F. H. Water molecule interactions. *J. Chem. Phys.* **53**, 4544–4554. https://doi.org/10.1063/1.1673986 (1970).

55. Xantheas, S. S. Ab initio studies of cyclic water clusters (H_2O)n, n = 1–6. II. Analysis of many-body interactions. *J. Chem. Phys.* **100**, 7523–7534. https://doi.org/10.1063/1.466846 (1994).

56. Sánchez-Sanz, G., Trujillo, C., Alkorta, I. & Elguero, J. Electron density shift description of non-bonding intramolecular interactions. *Comput. Theor. Chem.* **991**, 124–133. https://doi.org/10.1016/j.comptc.2012.04.007 (2012).

57. Iribarren, I., Sánchez-Sanz, G., Alkorta, I., Elguero, J. & Trujillo, C. Evaluation of electron density shifts in noncovalent interactions. *J. Phys. Chem. A* **125**, 4741–4749. https://doi.org/10.1021/acs.jpca.1c00830 (2021).

58. Jiang, B., Zhang, Q. & Dang, L. Theoretical studies on bridged frustrated Lewis pair (FLP) mediated H2 activation and CO$_2$ hydrogenation. *Organ. Chem. Front.* **5**, 1905–1915. https://doi.org/10.1039/C8QO00192H (2018).

Acknowledgements

Author contributions

M.F. did the calculations and the first draft of the article with contribution of the rest of the authors, I.A, J.E. and J.M.O.E., and reviewed and approved the article.

Competing interests

The authors declare no competing interests.

Additional information

Supplementary Information The online version contains supplementary material available at https://doi.org/10.1038/s41598-023-29336-y.

Correspondence and requests for materials should be addressed to I.A.

Reprints and permissions information is available at www.nature.com/reprints.

Publisher's note Springer Nature remains neutral with regard to jurisdictional claims in published maps and institutional affiliations.